2013

Investigation of microscale particles using a microfluidic flow cytometer equipped with a sensitive photodetector

Pouya Asrar
Iowa State University

Investigation of microscale particles using a microfluidic flow cytometer equipped with a sensitive photodetector

by

Pouya Asrar

A thesis submitted to the graduate faculty

in partial fulfillment of the requirements for the degree of

MASTER OF SCIENCE

Major: Mechanical Engineering

Program of Study Committee:
Nastaran Hashemi, Major Professor
Terrence Meyer
Liang Dong

Iowa State University

Ames, Iowa

2013

TABLE OF CONTENTS

LIST OF FIGURES

LIST OF TABLES

ACKNOWLEDGEMENT

I would like to express my deep gratitude to my advisor, Dr. Nastaran Hashemi, for her ever-present support, advisement and encouragement. It was a great experience to work with her and I obtained a lot of foundings from her at both professional and personal levels. I am also thankful to my other committee members, Dr. Terrence Meyer and Dr. Liang Dong for their support and comments.

Many friends have helped me during my graduate study. Their warm support and care assisted me to overcome obstacles and stay focused on my graduate work. I significantly value their friendship and I deeply appreciate their belief in me.

Most importantly, none of this would have been possible without the love and patience of my family. My parents, Manije and Ahmad to whom this dissertation is dedicated to, has been a constant source of love, consideration, support and strength all these years. My sister and brother, Pariya and Pouriya have aided and encouraged me throughout this endeavor. I would like to express my heart-felt gratitude to my family.

CHAPTER 1. INTRODUCTION

1.1 Motivations

Flow sorting could be accomplished by passing the particles through an electric field in the channel. A newer version of analysis uses different types of actuators cooperated with the flow cytometer for sorting the samples. When the flow sorting comes to mind, different cellular parameters might be accompanied without physically isolating the cells.

A flow cytometer works like a microscope to look at the small particles, but in terms of optical properties of them for further characterization. In fact illuminating the cells is done by the laser beam, this could be an analogous of what light source does in optical microscope to illuminate the specimen. The collected light enters a photodetector unit to produce a signal associated with the collected light. Producing a precise measurement of the signal is done by electronic devices like data acquisition means. When the illumination optics are accurately aligned and correctly focused, the appropriate signal will then produce.

The energy of the photon is inversely related to the associated wavelength. Interacting photon and electron causes scattering. In fact, the photon transfers its energy to an electron. This means that the light scattered by an object release the same energy in the same wavelength as the source light. Different reflectivity as well as different wavelength of coming light from the objects determines the contrast between objects. [1]

Particles have scattering which occurs in a small angle (usually between 0.5° to 5°) depending on the refractive difference between the particle and the medium and also the particle

size. Sometimes this forward scatter light uses to predict the size of particles. Small particles reflect more light as scattering light in bigger angles like 15° to 150° to the incident light. This kind of beam is called side or wide angle light scattering.

Depending on what kind of laser (wavelength) is being worked, different types of samples could be detected. Different particles send out different wavelength as an emission wavelength.

As the numerical aperture of the objectives and microscope devices, it is the maximum angle that they can gain or deliver the light.

In a medium that the samples are presented, some of the emitted light gets absorbed. In a solution containing samples, different areas become created in terms of the range of the wavelength that is transmitted from them. This scenario is the same for cells as they have pigments which make their surface to be distinguishable from the background.

1.2. History of Cytometry

In early twentieth century, light microscopy concepts especially in histologic staining techniques proved that tumors might contain abnormalities in DNA and RNA contents. Torbjorn[2] worked on development of some sophisticated micro spectrophotometers to have an accurate measurement of DNA and RNA contents based on UV strength of absorbed UV light near 260 nm. The first micro spectrometer was made of a field stop on which a small “pinhole” was designed to confine the view path to the area of a single particle (cell). There was also a photodetector located behind the field stop. The diameter of the field stop was based on the diameter that the measurement was going to take place using an optical lens. Using a 40

micrometers field stop it was possible to detect the samples as small as 1 micron. This structure could be mentioned as the only possible approach to scanning cytometry.

By that time, there was not any computer based data gathering system to capture the data. It was possible to take a lot of time to have high resolution scanned image from the samples. Higher scanning method was by using some moving mirrors designed in a galvanometer. It was around 1950's that someone investigated about bringing automated method of the process of looking under microscope and studying the samples using video processing. That was the time that image processing cytometers were introduced. The processors were fast as tens of kilohertz and memory storage devices were not large as couple of thousands kilobytes. This caused the process of data acquiring slow, so large amount of data were not possible to be stored. About a decade later on, attempts were focused on making commercial version of micro spectrophotometers to proceed analyzing through an automatically and faster path. This version was firstly introduced by Zeiss Company. During World War II, the United States needed to develop the evidences that could detect the bacteria as samples very rapidly in a volume of sample. This was more necessary than having a high resolution scanning medium. The unit was introduced on behalf of this necessity, injected the air stream including the samples into a sheath flow of air to focus the samples in core flow as much as possible to the center of the area. Then the samples were passing a focal point which was a dark-field microscope. The particles that were passing within the system scattered the light through an optical system consisted of arrays of lens. Then they would produce a signal as the output of a photodetector. This system is recorded to be as the first flow cytometer which was used to observe some biological cells. The particles were on the order of 0.5 microns in diameter. By early 1950's, the same method (Using sheath flow to protect the core flow) was used to count red blood cells floating in a sheath flows

which was saline solutions. This device was a big step in making a diagnostic testing system through an automation process instead of using a counting chamber to perform the test by a human observer. Discriminating the different types of samples was not feasible by that time as a quantifying measurement. In 1950's another method was introduced as an alternative for cell counting process by Wallace Coulter. He recognized that cells are not powerful enough in conducting electricity as they are surrounded by lipid members. He designed a space consisted of two chambers having an orifice in between that could pass samples as small as 100μm. The device was able to count the samples one by one because of change in volume of the chamber when once sample was passing through the chamber. A DC electric current was running across the orifice. In the early 1960's, an image analysis system was introduced to read the results of Papanicolaou smears that had been gained in the late 1950's. IBM transferred all the tasks of this image analyzer program to Louis Kamentsky as he had developed a promising optical character reader by then. Kamentsky[3]then concluded that the system couldn't respond all requests of image analysis concepts. Kamentsky then traveled to Caspersson's laboratory in Stockholm to learn micro spectrophotometry basics.

As a result, he came up with a flow cytometer to apply it as a device to estimate cell size. All cytometers by this time were able to analyze hundreds of samples, but not with a high performance in data acquiring. Scanning cytometry opened a new window for having a high data acquisition rate to apply in clinical purposes. Scanning systems comes with a controlling unit which is basically a computer that is programmed to reposition the cell throughout the view field of objective for identification by kind of visual observation. At first, it was impossible to distinguish cells based on the recorded characteristics from a flow cytometer. This issue was obviated in the mid of 1960's by introducing cell sorters by Mack Fulwyler and Kamentsky at

IBM. Kamentsky applied the cell sorter in his flow cytometers by using a syringe pump to extract desired samples from the running sample flow. Fulwyler used the concept of ink jet printer technology which consisted of a saline sample flow that reduced the size of the flow till droplets remain. These droplets contained the cells, and then they were charged by electrical circuit. Having the charged solution in presence of an electrical field, the droplets went as the selected cells.

As an improvement in quality and quantity of flow cytometry analysis, fluorescence measurement was introduced in the late 1960's. At the time three scientists, Van Dilla and Dittrich and Gohde [4-8] had reached to fluorescence based flow cytometry to measure the cells in DNA contents. Kamentsky found a center to produce the first commercial version of fluorescence flow cytometers. He incorporated an argon ion laser that was built by an arc lamp illumination that had a fluorescence microscope around itself. Another research group at Stanford realized that fluorescence flow cytometry which comes with cell sorting could be a promising method to study further on purifying living cells. They had problem with their old-fashioned illumination system, so they used a water-cooled argon laser as a more sensitive system of sorting cells from the immune system. So, by 1979's flow cytometers were being produced which were able to record results with thousands cells per second rate and capability of recognizing large and small scattering angels in the minimum of two wavelength zone. This achievement happened when breast cancer and other malignancies were being brought to attention.

Fluorescence and flow are engaged for flow cytometry application, but fluorescence comes with inconsistent measurement while flow doesn't. When an atom or molecule absorbs a

photon, the corresponding electron to that energy will raise its level to an excited level. Part of this energy could be lost as heat or other forms of energy; the remained package of energy is then emitted with a longer wavelength(less energy of photons) as fluorescence. At some points, the fluorescence will not be excited; instead photobleach which is a fluorescence molecule will result in a non-fluorescent package by breaking of chemical bonds. This phenomenon happens after having little number of excitation and emission out of each cycle of fluorescent.

The intensity of fluorescent of the materials that are being observed is basically related to the concentration of them in the area. In an unsuccessful attempt in 1930's, it was tried to realize the antibodies were attached to cellular structures, but as the background field was bright, it was not possible to receive the different organic dyes attached to antibodies.

The fluorescence measurements are generally more sensitive to absorption measurements. This would be as positive point in detecting smaller field of view. Also different types of cells are easier to be measure through fluorescence rather than absorption. This process is then called multi-parameter cytometry.

Investigation of selected particles in a solution using a cytometer requires a reasonable range of resolution. For example, having detected 3,000 samples out of 30,000,000 samples that most of them are almost the same in terms of fluorescence property need a high-speed capacity of recording data. The data become recorded by data acquisition device which is linked to the flow cytometry system. The can record data from samples in an expanded range. Higher frequency of data acquisition system would cause higher resolution of the system.

1.3. Outline

A summary of next chapters are as follows:

Chapter 2: The optical and electronics systems are completely explained. Alignment of different optical elements as well as setting the electronic unit of the system is purely discussed.

Chapter 3: The simulation part of the project using the COMSOL software is studied. Designing the 3D geometry of the microfluidic device is figured out. The velocity and concentration distribution along the channel is computed and plotted on graphs.

Chapter 4: We discuss about employing a very sensitive with high resolution photodetection unit which is called MPPC. Using MPPC, two different sizes of samples are detected by our flow cytometer. Further analysis on the signal output from the system is investigated and statistical results are presented.

Chapter 5: Conclusion and future studies are presented.

1.3. References

[1] Howard M. Shapiro, Practical Flow Cytometry, fourth edition, 2003.

[2] Caspersson TO: Cell Growth and Cell Function. New York, Norton, 1950.

[3] Kamentsky LA, Melamed MR: Spectrophotometric cell sorter. Science 156:1364, 1967

[4] Van Dilla MA, Trujillo TT, Mulancey PF et al: Cell Microfluorometry: A method for rapid fluorescence measurement. Science 163:1213, 1969.

[5] Evans DMD: Cytology Automation. London, Livingstone, 1970.

[6] Saunders AM, Hulett HR: Microfuorometry: Comparison of single measurement to a rapid flow system. J Histochem Cytochem 17:188, 1969.

[7] Hulett HR, Bonner WA, Barrett J et al: Automated separation of mammalian cells as a function of intracellular fluorescence. Science 166:747, 1969.

[8] Dittrich W, Gohde W: Impulsfluorometric bei Einzelzellen in Suspension. Z Naturforsch 24b:360, 1969.

CHAPTER 2. OPTICS AND ELECTRONICS

2.1. Introduction on Optics and Electronics

Talking about an optical system, we first should focus on an origination point of light which is called point source. Rays of light come out of the source in all directions. They become farther from each other as they go further away the point source and along a direction. In fact, the rays are divergent in nature. They are also called negative vergent. As they become parallel in direction, they would get zero vergence property. They rays that are all in parallel direction, they called collimated rays. There are also convergent rays that become closer and closer as they go along a direction. All the rays go straight in terms of direction except the one which are reflected or refracted. Those which are refracted are shared in a specific optical property which is called index of refraction that determines at which angle the light bends between two areas of work. The refractive index is called by n. If a ray travels along a direction for a distance of "X" in a medium that has refractive index of "n", a property that is called optical path length could be defined as S = Xn which indicates amount of the length that a light could travel in a vacuum condition. The time frame for both cases is assumed to be the same. In order to provide a precisely focused light through an optical system, different elements such as optical fibers, lenses and lasers should be employed in the setup.

The lasers are sources of light in a broad range of wavelength that is used in optical system to provide the desirable amount of light. The lenses are the other optical items that are made of glasses or plastic material that are responsible for providing a set of rays in a specific form. The distance in between the light source and the lens is called the focal length of the

system. For example, in the current project, a diode laser is used to provide the source of light in the system which has parallel rays of light coming out of it. Also, an objective lens is used in front of the laser to produce sets of rays that are perfectly focused in a very tiny point. So, the laser and the objective lens make a planar optical system which means that the rays are traveling in between these two elements are parallel. Once the rays travel through the lens they become converged and make the converged rays of light in a focused light spot. Around this sport there are little rings that indicate an image of the distant point source. These kinds of rings are called diffraction rings. The lenses that provide these types of shapes are called diffraction limited lens which is an opposite of aberration limited lens. This spot can provide input light for other optical elements such as optical fibers.

The first thing in an electrical system that comes to mind is the electrons and protons that are involved in the system as the main parts of the system. The electrons basically travel around the protons. They carry the negative charge, in contrast with the protons which have the positive charges in an electrical system. The unit of charge which is indicated by "q" (coulomb) is about 1.6×10^{-19}C. Electric field is produced by separation of charges through a medium. This field makes the charges to have more potential energy. For example, for two plates that are charged with opposite charges, the field extract the electrons and make them attracted by the positive plate. These electrons then have potential energy which degrades as they become closer to the positive charges. (lower level of potential energy). This potential energy is proportional to the charge of electrons. The potential difference in an electrical system between two points is defined as 1 Volt (V). If the travelling of charges is operated through conductors, this transfer makes the electric current. Based on this electric current, transferring of 1 coulomb of charge per

second represents 1 ampere (A). In fact the electric current is a force that is produced through the positive side and attracts the electrons towards the positive position.

A resistance is a drop in voltage potential or electric current in the system that is defined by "R" (ohms, Ω). The resistors are the elements that play this role and follow this equation:

$$V = IR \quad (1)$$

The currents are produced through DC (Direct Current) and AC (Alternating Current) sources. The DC sources produce a consistent flow of current through system, but the AC system produce the oscillating function of current as an output. In this project, all items are supported by the DC sources. The power sources that produce DC currents are called DC power supplies. In all parts of the experiments in this study, DC power supplies are introduced in the system to produce direct current through wires.

In flow cytometry, data acquisition devices (DAQ) have a significant role in obtaining data from the samples that run through the system. These electronic devices have data rate as one of their specifications that indicates how fast the data are obtaining from the samples per unit of time. Higher data rates indicate higher capacity of DAQ system to obtain the data. One type of the data acquisition units is the DAQ boards that are made of some analog input and output terminals. Depending on the number of analog input of the board, the number of independent signal input could be determined. In fact, in a flow cytometry system, there could be as much as channels to release the data as the number of analog input terminals.

2.2. Laser, Fiber and Lens Adjustment

To obtain the maximum intensity of the laser beam, all optical elements should be adjusted (aligned) with each other. In fact, they are all supposed to line up together. First, the laser is installed on a holder and is connected to the optical table. Using an iris, the laser beam is aligned in 2 different locations. Then, the lens is set in front of the laser. Using a paper the beam coming from the laser is fixed at the very center of the lens outlet. This is the only way that we can expect to have the most intensive light going through the fiber. Using a micro positioner, the light coming out of the lens is exactly positioned at the center of the single mode optical fiber. This fiber takes the role of excitation fiber. Details on the optical system training is completely explained in the next section. We were able to meet 2 μ W as the maximum power coming out of dump fiber through the mentioned method. This is a very narrow region in gaining the maximum power from the laser. This is because we have used the single mode fiber as excitation fiber and its core diameter is just 9 microns. The laser that is utilized in this section has 10 mW as its maximum power output. Figure 1 shows a schematic of flow cytometer.

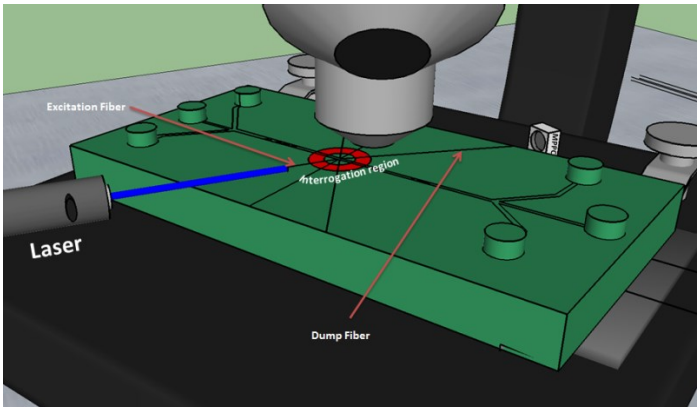

Figure 1. A Schematic of the Flow Cytometer. The excitation and dump fibers are shown.

2.3. Lens Selection

Having a perfectly focused light through the optical fibers, a lens is required. In this project an objective lens is used to focus the light into the core part of the optical fiber. Lens could be selected by calculating some equations that are involved with different parameters of the optical elements. In the following sections, it is completely explained how the correct objective lens is picked up.

2.3.1. Numerical Aperture

Before starting the calculations for selecting the correct lens, the numerical aperture is explained here which is one of the specifications of the optical fiber.

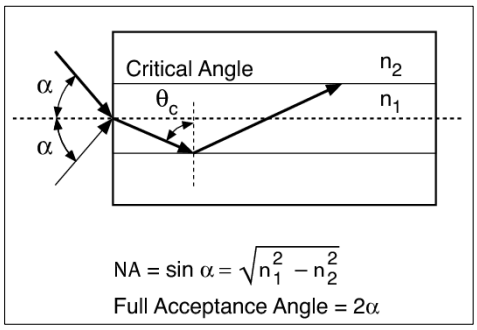

Figure 2. Schematic of incident light through optical fiber core

The numerical aperture or N.A of a fiber is the sin of the angle of incident light. This could cause total reflection through the core of the optical fiber. The highest quality of aligning the light through the fiber core happens when the N.A gets to its maximum possible point.

In fact the diameter of the light coming out of the lens should be equal or a bit larger than the core diameter of the optical fiber. We have used a single mode fiber as the excitation fiber. The core diameter of the fiber used in this project is 9 microns. That is a single mode optical fiber. Using the core diameter of the fiber and the wavelength of the light shooting through the fiber, the objective lens could be selected.

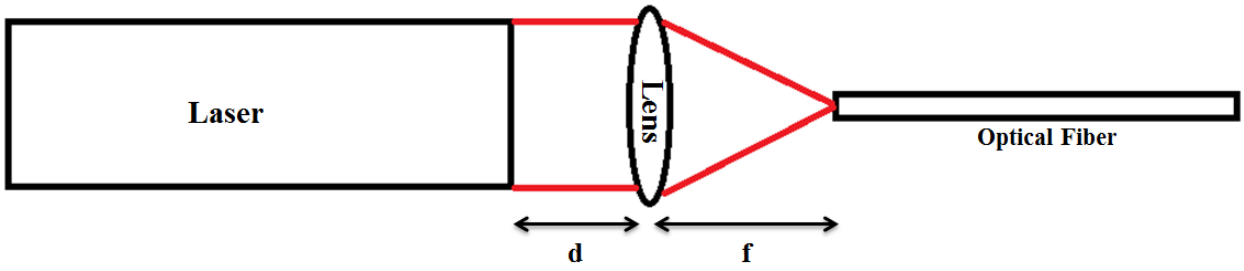

Figure 3. Schematic of Optical Training

Figure 3 shows a schematic of the optical system training which is consisted of laser, lens and the optical fiber. First of all, using iris the laser and lens are precisely aligned with each other. These two elements make a planar system which means that the rays that are coming out of laser are parallel to the horizontal axis of both laser and lens. Then, the objective lens is responsible for focusing the beam of laser at a very confined point. The optical fiber should

exactly be mounted at that point to receive the maximum intensity of the light through the core. Having the core diameter of the fiber, the focal length could be calculated by the following equations and finally the correct type of objective lens could be selected. In figure 3, f is the focal length of the lens which could also be determined by the experimental procedure. This could be done by using a paper, while laser beam is shining through the objective lens, Making the optical fiber closer or farther of the lens, a point could be found that the most focused and the highest intensity of the light could be obtained, Once the fiber is fixed at that location, the distance in between the lens and fiber indicates the focal length of the lens.

2.3.2. Calculations for Selecting an Appropriate Objective Lens

First the V factor should be calculated through following equation:

$$V = 2\pi . NA. a/\lambda \quad (2)$$

Where V is the Normalized Frequency Parameter of fibers, NA is the numerical aperture of the lens and a is the radius of the fiber core. The λ stands out as the wavelength of the light.

Using the above equation, the Gaussian distribution for the fiber could be calculated by the following equation:

$$w = 0.65 + \frac{1.619}{V^{1.5}} + \frac{2.879}{V^{6}} \quad (3)$$

Having w, the beam diameter (D) could be obtained by:

$$D = 4\lambda f/(\pi w) \quad (4)$$

Having the wavelength of the light, the V number could be calculated. The core diameter of the fiber and the numerical aperture are assumed to be 9 microns and 0.1, respectively. Having V number, w could be obtained by equation (3). Finally the focal length of the lens is determined by equation (4). , according to equations (2)-(4), for the $\lambda = 635$ nm, V, w and D are calculated as 0.453, 0.17 and 3.2 mm, respectively. Finally by calculating the focal length of the lens the appropriate lens is selected. In our project, the objective lens MV-5X is selected from Newport Inc. The focal length for the mentioned lens is 25.8 mm.

The following table shows how changing the wavelength of the incident light can affect the focal length of the lens.

Table 1. The effect of wavelength on focal length of lens

λ (nm)	V	w	f (mm)
635	4.453	0.173	25.8
532	5.315	0.132	23.5
405	6.98	0.088	20.5

Table shows that by decreasing the wavelength (and decreasing w accordingly) of the incident light the focal length of the lens decreases.

2.4. Optical Fiber Selection

2.4.1. FC Connector Fibers

This type of connector for fiber is used for single mode fiber applications. The connector is made of ceramic ferrule that is equipped with an anti-rotation key. This key helps to have higher alignment of fiber as well as it increases the durability of the connector.

For all the experiments, the FC connector fiber is used as excitation fiber in the setup. The core diameter of this type of fiber is 9 microns. Figure 4 shows a FC connector.

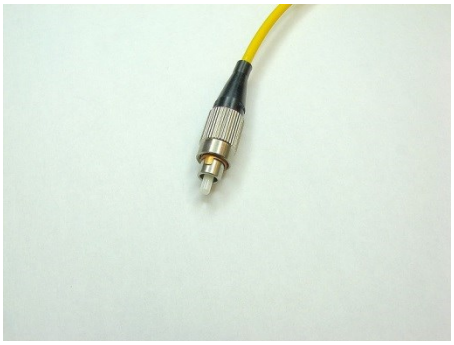

Figure 4. FC Connector

2.4.2. ST Connector Fibers

The multimode fibers are also utilized as emission fibers in the system. The multimode fibers have ST connector. ST connectors are almost the same as FC connectors except the push-pull mechanism that is added in this type for easier aligning the fibers in the optical system. The core diameter of this type of fiber is 65 microns. Figure 5 shows the a ST connector.

Figure 5. ST Connector

2.5. References

[1] Howard M. Shapiro, Practical Flow Cytometry, fourth edition, 2003.

[2] Tutorial on Optical Elements available on Newport company website.

CHAPTER 3. COMSOL SIMULATION

3.1. Introduction

The COMSOL Multiphysics is used to create the 3D geometry of the microchannel. We have developed the simulation based on two different aims: one is obtaining the velocity distribution along the channel using Navier-Stokes equation. As the next step, we have used the results of the first step and have come up with the simulation for the concentration distribution along the channel using the Fick's Law. For the first step, the Laminar Flow version and for the second step the Transport of Diluted species on COMSOL is utilized. The time of running simulations for each step is dependent to the quality of mesh that is defined.

3.2. Parameters

The general parameters of the simulation by COMSOL are defined as following:

Table 2. The general parameters of the simulation

Name	Expression	Description
D	1e-9 $[m^2/s]$	Diffusion Coefficient
c0	1 $[\mathrm{mol/m^3}]$	Concentration of Samples
QCore	2.5e-6 [L/min]	Core Flow Rate (10uL/min)
QSheath	50e-6 [L/min]	Sheath Flow Rate (200uL/min)
rho	1e3 $[\mathrm{kg/m^3}]$	Density
eta	1e-3 [Pa. s]	Dynamic Viscosity

3.3. Geometry

The figure 1 shows the geometry of the channel. As shown in the figure below, only forth of the channel is designed for the simulation to shorten the time of the channel simulations. This means that the results are as a part of a symmetric result of the whole channel. The chevron grooves have 65 microns height above the channel. The height of the shown channel is 65 microns (half of the whole channel height). The width of the designed channel is 195 microns. The length of the simulated channel is about 15 mm. First, a plane is selected to draw the 2D version of the channel. XY plane is chosen as default for this purpose. Then the rectangle is extruded along the Z-axis to make the 3D shape of the whole channel. The 2D chevrons are designed on the top of the 3D channel. Using extrusion the 3D chevrons are made on the top of the 3D channel for 65 microns in terms of the height. The distance in between the chevrons is 100 microns. The figure 1 shows only one fourth of the whole channel. A plane is defined on y-z plane at the inlet location. The purpose is to design the core and sheath inlets. The core inlet and sheath inlet width are 20 and 175 microns, respectively. After designing all the elements of the microfluidic design, all separated parts such as chevrons, inlets, and the main channel are made as a single rigid body using the union option of the COMSOL. This was because of having the simulation for the whole design run at the same time. The interior boundaries are also checked off to have the whole thing as a single geometry.

3.4. Fundamental Background of COMSOL Computations

The results are velocity and concentration distribution along the channel. To get to this aim, the Navier-Stokes and the Fick's law are solved.

$$\rho\left(\frac{\partial u}{\partial t} + u.\nabla u\right) = -\nabla p + \rho g + \mu \nabla^2 u \quad \text{(Navier-Stokes Equation)} \tag{5}$$

$$\nabla . u = 0 \text{ (Continuity Equation)} \tag{6}$$

$$J = -D\nabla C \text{ (Diffusion Equation-Fick's Law)} \tag{7}$$

Where ρ, u, p, J, D and C are the density, velocity, pressure, diffusion flux and the concentration of the fluid that is being studied.

$$Re = \frac{Vd}{\eta} \tag{8}$$

Equation (8) is the Reynolds number equation where V, d and η are the fluid velocity, diameter of the observation section and dynamic viscosity of the fluid, respectively. The velocity of the fluid is 65.7 mm/s and the equivalent diameter of the channel cross section is 240 microns. Also the dynamic viscosity of the fluid is .001 Pa.s.

The flow in the channel is assumed to be at steady state condition with laminar regime. Therefore the Reynolds number is calculated to be 31 during the process.

The discretization method in solving the equations for pressure is defined to be as second order. In fact, the pressure distribution is defined as a second order function instead of linear trend. In the P2 + P1 scheme a second order (quadratic) shape function is used to calculate the velocity distribution, while a linear shape function is used to calculate the pressure distribution. This scheme works best for low flow velocity situations. In the P1 + P1 scheme, a linear shape function is used to calculate both the velocity and pressure distributions. This scheme is the computationally cheaper of the two and is less prone to spurious oscillations which improve the numerical robustness of this scheme. Because of symmetry property of the geometry, some of

the walls are defined as symmetric planes. The inlet section is defined as velocity inlet and the outlet is set to pressure driven. The rest of the areas are set as regular walls.

The core flow is supported from one of the sides of the channel by sheath flow. The concentrations of sample and sheath streams are set to 1 $^{mol}/_{m^3}$ and 0 $^{mol}/_{m^3}$. The fluids are assumed to be as incompressible fluids. The microfluidics module on COMSOL is used for running both velocity and concentration simulation parts. For the concentration solution, Transport of Diluted Species part of the COMSOL is employed to solve the quadratic function for the concentration distribution along the channel.

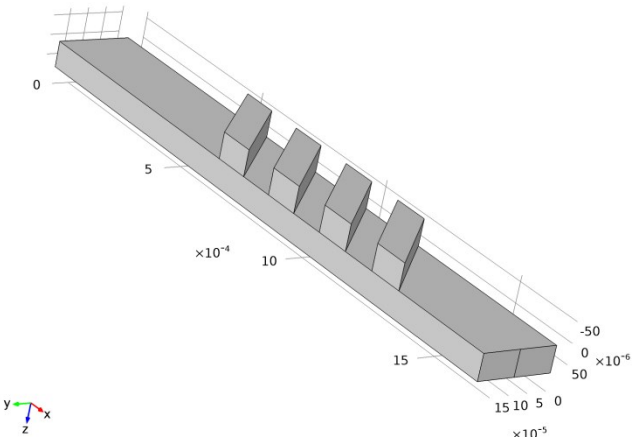

Figure 6. The 3D Geometry of one-fourth of the microchannel

All the fluid flows are defined as laminar flow condition because of the low velocity and the low range of the Reynolds number.

3.5. Computations

3.5.1. Laminar Flow Computations

The first set of computations solves the Navier-Stokes and continuity equations to finally obtain the velocity results for the whole 3D geometry. In fact the velocity distribution along the channel could be shown on plot section of the software by having the data points of velocity components in x,y and z as the coordinate system. u, v and w are set as components of velocity of fluid field along the x, y and z axis, respectively. p is also the pressure field that is defined for the fluid streams in all sections.

$$\rho\,(\mathrm{u}.\nabla)\mathrm{u} = \nabla.[-\mathrm{p} + \mu\,(\nabla\mathrm{u} + (\nabla\mathrm{u})^{\mathrm{T}}] \tag{9}$$

$$\rho\,\nabla.\mathrm{u} = 0 \tag{10}$$

Equations (8) and (9) are the Navier-Stokes and continuity equations along x axis, respectively.

3.5.2. Wall 1 Geometry

Wall 1 is the whole 3D body that contains all the vertical and horizontal planes that are become as a single rigid geometry using the union option on COMSOL. The figure 2 shows one-fourth of the 3D design of the channel by COMSOL software.

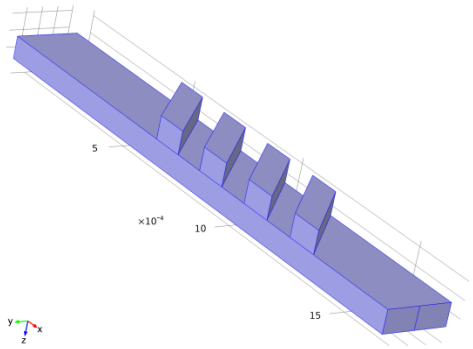

Figure 7. The whole channel wall

In all parts of the simulation, the flow condition is set to be laminar and the core and sheath flows are defined as Q_{core} and Q_{sheath}.

3.5.3. Outlet Conditions

There is only one outlet defined in the design by COMSOL. Following equations are defined for outlet of the microchannel:

$$p = p_0 \tag{11}$$

$$[\mu(\nabla u + (\nabla u)^T] \,.\, n = 0 \tag{12}$$

According to equations (1), (2), the velocity field is set at zero and the only parameter that is making role in the outlet is the pressure. Equation (12) shows that there is no velocity field coming out of the outlet (pressure condition perpendicular to the outlet plane).

3.5.4. Symmetric Walls

Since only one fourth of the channel is studied for the simulation, the side wall and the bottom wall of the channel should be assumed as the symmetric walls in the design. In fact by making these walls as symmetric, they have the same condition as other solid walls in the geometry (no flow condition).

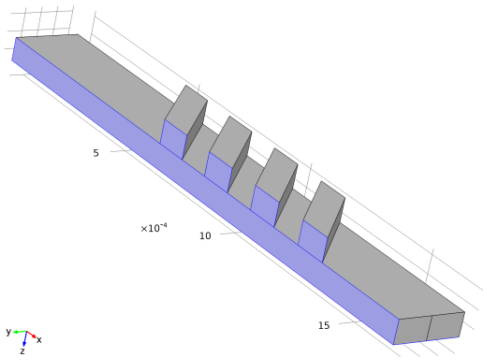

Figure 8. Symmetric wall of the channel

The following equations are defined for the symmetric plane to be computed through the simulation process:

$$u.n = 0 \tag{13}$$

$$K - (K.n)n = 0 \tag{14}$$

Where K is as follows:

$$K = [\mu(\nabla u + (\nabla u)^T]n \tag{15}$$

The equations (13)-(15) indicate that the velocity field perpendicular to the symmetric plan is zero and there is no flow coming out of the side plan of the channel. In fact this wall has the same condition as the other wall that are defined as solid walls (no flow condition).

3.6. Transport of Diluted Species Computations

In order to obtain the concentration distribution along the channel, the Transport of Diluted Species section on COMSOL simulations should be applied. This part starts computing the equations using the results that are obtained by the first section of computations after computing the first step of the results which is velocity distribution along the channel.

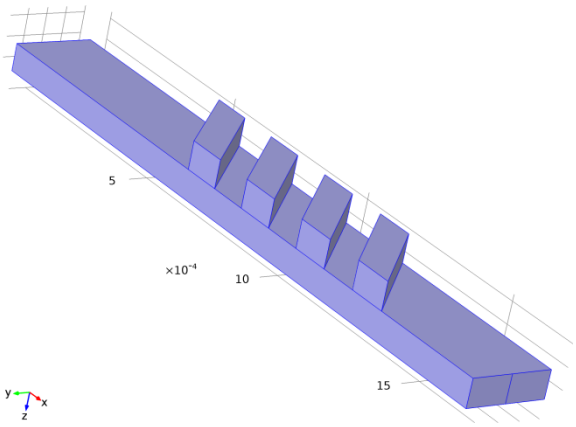

Figure 9. The geometry defined in Transport of Diluted Species

$$\nabla.(-D_i\nabla c_i) + u.\nabla c_i = R_i \quad (16)$$

$$N_i = -D_i\nabla c_i + uc_i \quad (17)$$

The equation (16) is the general equation of diffusion where c is the concentration property and R is the sink or source of the quantity c. Depending on the chemical reactions that occure for chemical species. For those reactions that produce more species, R is positive. In contrast for the reactions that destroy the species R is negative. In the calculations of this section, R is zero as there is no chemical reaction occuring in the channel.

Equation (17) is the advective-diffusion equation whre N_i is the total flux. The first term on the right side of the equation is the first Fick's law or diffusive flux equation. This term is related to the diffusion flux of material (bulk motion of particles) which is completely dependent to the local concentration gradient. The second term is called the advective flux which comes from the overall convection of the fluid flow.

3.6.1. Concentration of Core Flow

The core flow concentration is set at $1\ {}^{mol}/_{m^3}$. The effect of this setting will be discussed in the results of concentration distribution along the channel.

3.6.2. Concentration of Sheath Flow

The concentration for the sheath flow is set at $0\ {}^{mol}/_{m^3}$. This is because we are going to distinguish between core and sheath flow. In this condition the only fluid that has concentration is core stream.

3.6.3 Concentration of No Flux Area

As mentioned earlier, the walls are assumed to have no flux condition except the inlets and outlet locations.

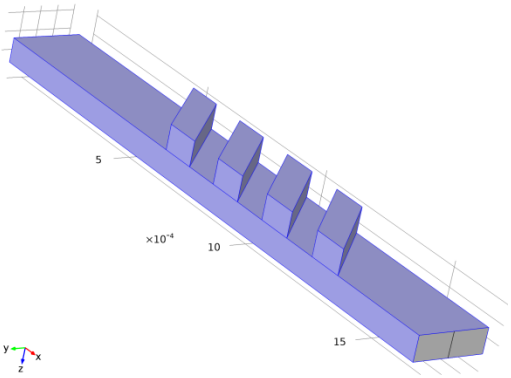

Figure 10. No Flux walls

For those walls that are assumed to be as rigid walls (no flow condition), the following equation is valid: $-n.N_i = 0$ (18)

Equation (18) approves that there is no flox out of the walls that are assumed to be as no flux regions.

3.7. Meshing:

In order to compute the equations though different sections of geometry, the software should detect the geometry. Then, it applies the proper equations for the selected part of the 3D shape. In order to get to this goal, a fine mesh should run within different horizontal and vertical planes in the geometry. For the studied channel, the horizontal and vertical planes are meshed with triangular and rectangular meshing, respectively. This because we can have a smooth connection at the edges and prevent errors in computation in those parts. The Distribution option is applied near the walls on the software. This option usually applies to the meshing when the boundary layers near walls are going to be studied. The whole meshing patter is called structured

mashing method. This meshed is in contrast with the regular meshing process (consistent size and shapes of the mesh). Figures (8) and (9) show snap shots of structured mesh for the whole channel and the around the chevrons grooves, respectively.

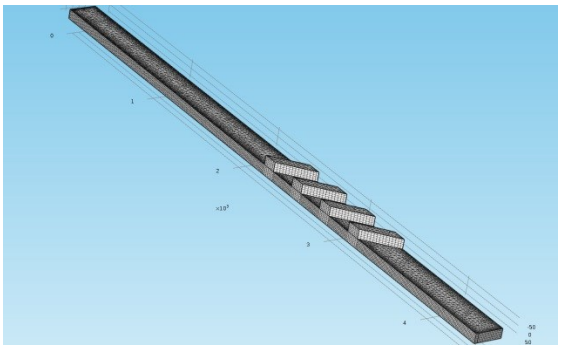

Figure 11. Meshing of the whole channel

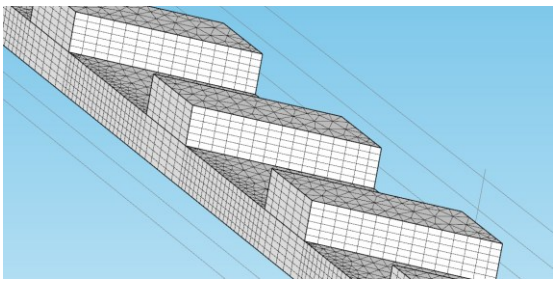

Figure 12. Structured mesh around the chevron grooves

3.8. Simulation Solvers

First, the program solves the Navier-Stokes equation. The results are saved by the software for the second step. In this step, the velocity distribution along the channel would be solved. Using the 3D plot option on COMSOL the distribution could be depicted. The figure 10 shows the velocity distribution along the channel in 3D mode.

The second run is dependent to the first step in terms of velocity values. At this point, the solver uses the velocity data points to get the concentration distribution along the channel as the second package of results. The figure 11 shows the concentration distribution along the channel in 3D mode. The meshes are run through extremely fine condition in all computation processes.

3.8.1. First Step: Navier-Stokes Equation Solver

The first step is running the program to solve the Navier Stokes and continuity equations to obtain the velocity distribution. Since the range of the fluid velocity in both streams (sheath and core) is not high, the regime of the flows is low Reynolds number. The Navier-Stokes equation in this regime is called Stokes equation.

In all equations, it is assumed that stationary (steady state) condition is valid. For the Laminar Flow calculations, the initial conditions are set at 0 (stationary). In the second step of the simulations which the Transport of Diluted Species equations would be run, the results of the first step is going to be used as the initial conditions of the second step to get the correct concentration distribution along the channel.

3.8.2. Second Step: Convection-Diffusion Equation Solver

In this part, the concentration distribution along the channel is obtained through the Transport of Diluted Species section in the simulation. The software utilizes the convection-diffusion equation to calculate the concentration distribution of the fluids along the channel.

3.9. Results

The results for both velocity and concentration along the channel are as following figures:

3.9.1. Velocity Distribution Plot

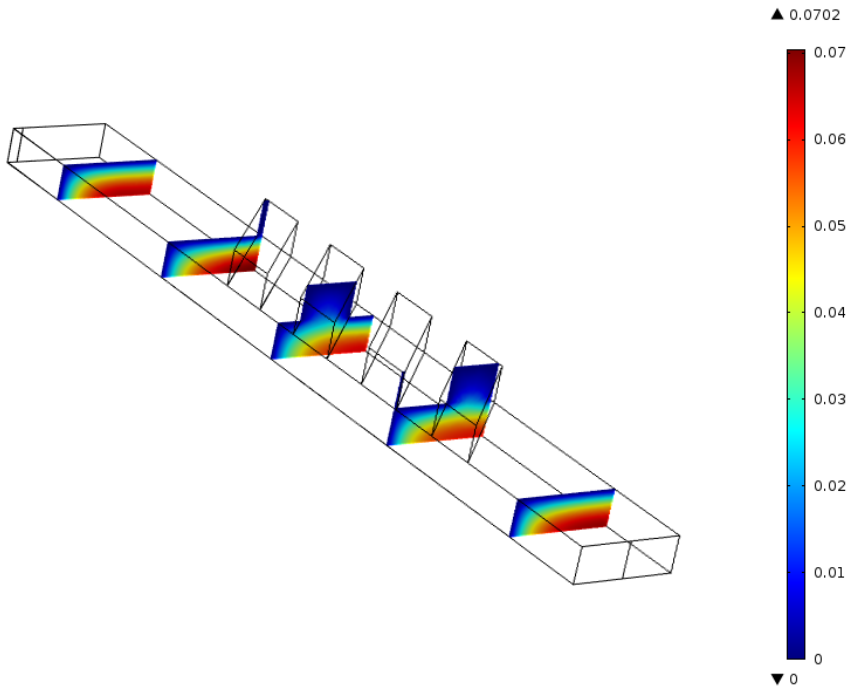

Figure 13. Velocity Distribution along the channel

Figure 10 Shows that near the walls there is almost no velocity involved with the flow. Instead for the locations closer to the center of the channel the velocity reaches to its maximum value (red zones). Figure 10 only shows the velocity results for one-fourth of the channel.

3.9.2. Concentration Distribution Plots

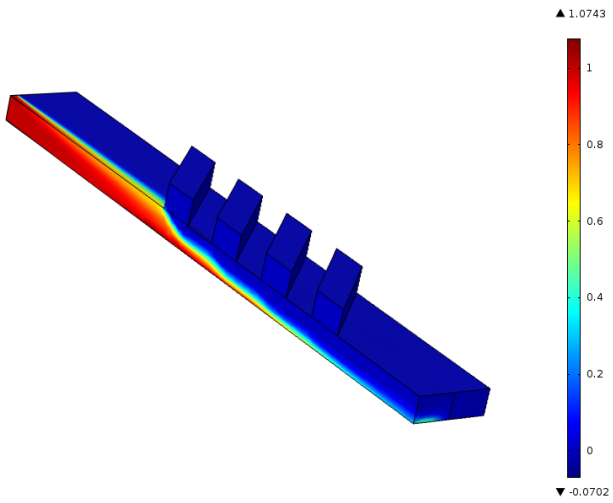

Figure 14. Concentration Distribution along the channel in 3D

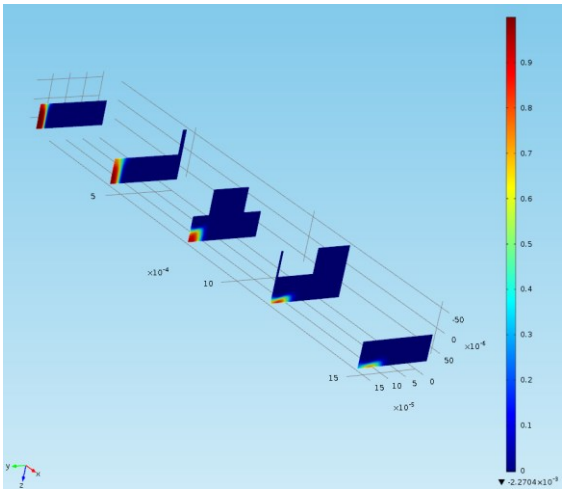

Figure 15. Concentration Distribution in across yz plane along the channel

Figures 11 and 12 show how the chevron grooves have made the core flow focused at a very compressed region at the center of the channel. The 3D dynamically focusing property of the flow cytometer is also detectable by figure 12. In fact, it proves how the chevron grooves and

sheath flow have made the sample stream encompassed across vertical and horizontal axes, respectively. The range of the concentration distribution proves that the maximum possible concentration that the fluid element could get is $1\frac{\text{mol}}{\text{m}^3}$.

3.10. References

[1] COMSOL 4.2a User's Manual

[2] Munson, Okiishi, Huebsch, RothmayerFundamentals of Fluid Mechanics

CHAPETER 4. OPTOFLUIDIC CYTOMETRY USING MULTI-PIXEL PHOTON COUNTERS

4.1. Abstract

We have developed a sensitive optofluidic cytometer to investigate microscale particles. The flow cytometer is comprised of a microchannel that has a set of chevron-shaped grooves. Conducted by the chevrons, two sheath streams focus the core stream in the center of the microchannel three-dimensionally. The optofluidic cytometer is equipped with the new generation of photodetectors, multi-pixel photon counter (MPPC). MPPCs are highly sensitive photodetectors with extremely small footprint that deliver high gain values of up to 10^7. We have employed a MPPC as the photodetector unit in our cytometer. Two different sizes of high intensity fluorescent microspheres are run through the cytometer. The signal outputs from both particles are collected using a data acquisition unit for further statistical analysis. The emission light produced by samples is received by a multimode fiber that is located in 135-degree with respect to the excitation fiber. The effect of particle size on the range of collected signal output is investigated by observing the forward scattering emission from samples. Statistical analysis of collected signal proved that for 10.2 μm particles, the peak height, width, and consequently area are larger than 3.2 μm particles. Finally using a 35 mW diode laser three types of algae are characterized in the flow cytometer based on their sizes. COMSOL software was employed to simulate the concentration distribution along the microchannel.

4.2. Introduction

Flow cytometry and particle detecting and sorting is receiving increasing research attention in recent years. In many sciences such as fluid mechanics and oceanography, it is needed to find a way for quantification of system particles [1, 2]. Many researches have put endeavors to move through a compact, low power consumption and cost-effective design. Heidi et al. worked on chlorophyll analysis using different types of flow cytometers to develop usage of portable particle counting device. Performance of such devices was highly dependent on the design of the microchannel [3]. Howell et al. used parallel stripe grooves on the surface of a channel with T-intersection inlet to conduct the sheath flow around the sample stream in the main channel. They found that by increasing the number of chevrons the height of the core flow has a decreasing trend. The limitation in the aspect ratio of the channel was a restriction point in their design [4]. Mao et al. developed a planar microfluidic device applying 3D hydrodynamic focusing concept. The portable device had a pattern consisted of four inlet channels to focus the core flow to the center of the microchannel and a single outlet channel. They performed the fabrication with a single layer microfluidic medium using soft lithography process. Their exclusive design which was called “microfluidic drifting” eased the process of fabrication of a portable flow cytometer which could make it possible to have 3D hydrodynamic focusing through the fluidic channel [5]. Golden et al. designed a device based on hydrodynamic focusing concept which had chevron-shaped grooves inside the channel to encircle and focus the core flow to the center of the channel. They also investigated the shape of the focused flow (sample) at different Reynold’s numbers in terms of the position of sheath and sample streams [6]. Hashemi et al. fabricated a microchannel with chevron-shaped grooves to perform 3D hydrodynamic focusing. Using this design, the sample (core) stream was enclosed with two

sheath flows compress it from top and bottom in chevrons locations. They were able to characterize microorganisms with a 1 μm in diameter [2]. They were also able to recognize a wide range of marine algae of various sizes using different types of lasers as excitation devices at different wavelengths [7].

Bernini et al. introduced a compact microfluidic device to detect the samples running through the microchannel. The design had a core and two sheath channels which were supposed to squeeze the core flow. A specific feature of this work was the geometry of the chip which was called antiresonant reflecting optical waveguides. This feature allowed having both sample flow and detection unit at the same channel. Also it reduced the signal-to-noise ratio level. The results obtained using their integrated microdevice was confirmed by a bench-top flow cytometer [8]. Guocheng et al. designed and fabricated a flow cytometer with 3D hydrodynamic focusing in the design of the channel. Having 30° slopes through the flow path, they were able to set the flow at the center of the stream channel. They also designed microlenses located out-of-plane of the stream channel to provide a completely focused light for the output optical fibers. The light coupling efficiency was calculated using software Zemax EE to determine the percentage of excitation light coming from the output fiber. They were then able to confirm their experimental results with the mentioned commercial software output. Guocheng et al. studied the coupling efficiency of two systems—one had a direct coupling system and the other had microlenses imbedded. Longitudinal offset and radial offset were studied for the light source. In spite of using the direct coupling system, the microlens-aided system showed sensitivity for both longitudinal and radial offsets [9]. Hairer et al. presented a microchip that included four sheath entries; three coaxial and one non-coaxial. They used one of the coaxial sheath ports as a lifting sheath port to conduct the sample stream in a narrow portion of their microchannel. The special

design of the sheath flows allowed having sample stream with desirable position wither horizontally or vertically. They were able to confirm this property of their design by CFD simulations. Using a confocal laser scanning microscope, it was feasible to characterize the sample flow profile conveniently [10].

Throughout all developments, the special need of having a novel design in photodetection part of flow cytometers attracted the attentions to have a simple and cost-effective but sensitive and strong optical unit like using cell phone devices. Tseng et al. utilized a imaging unit which was attached to a cell phone as light source platform. In fact, this study described a novel way of having a microfluidic setup without incorporation of bulky optical elements such as lenses and lasers. They assessed the performance of their imaging device using different microscale samples and red blood cells. Tseng et al. modified the images captured by the cell phone camera using digital processing [11]. Zhu et al.'s designed a cell phone-based flow cytometer which was compact and light to analyze white blood cells with different densities. Their imaging unit that was a cell phone camera was perpendicularly positioned to the flow path. This approach caused a proper and continuous visualization of the samples which are running through the microchannel. They introduced an external spherical lens and absorption filter to set the fluorescence light coming from samples to desired wavelengths [7]. Zhu's group were able to quantify the density of white blood cells within 30s time frame. Their imaging unit had the capability of reaching 2 μm in terms of florescent resolution. They finally verified their results with a commercial flow cytometer that demonstrated a 95% match to each other [12].

Kostner et al. analyzed biological cells using a flow cytometer equipped with a DVD pick-up head to support the detection section of the setup. A mirror was place at the bottom of the flow channel to reflect the beam of the laser through the photodiodes. This special feature

made the device very sensitive for the sample counting. To ensure the beam's profile, Kostner et al. placed a detector array at the bottom of the optical design to check the shape of the reflected beam. Their design eliminated the adjustment problem between the laser diode and the photodiode in the detection area. They introduced both polystyrene beads for testing, and erythrocytes as the nominated samples in the microchannel. They were able to show the efficiency of their design in separation and counting a mixture of beads in the channel. The cells were out-of-focus at some point, which affected the sensitivity of the reflected intensity [13]. Mao et al. fabricated a flow cytometer which was able to both focus and detect the particles which were running through its microchannel. The flow cytometer was designed based on microfluidic drifting capability which allowed having 3D hydrodynamic focusing in the channel. The design had a 90° corner to focus the particles at the center plane of the stream channel. There was a side sheath flow channel to ensure alignment of the particle in a single line. Mao et al. collected three types of output signals simultaneously: forward scatter (FSC), side scatter (SSC), and fluorescence (FL). To this end, they employed a single-mode of optical fiber for excitation light and three multi-mode optical fibers for FSC, SSC, and FL collections. Photomultipliers were used to detect the signals and they were able to adjust to desirable gain. Mao et al. compared their results with a commercial flow cytometer Beckman-Coulter FC500. They tested two particles and presented 3D graphs for Forward and Side Scatters versus Fluorescence for both commercial and their own flow cytometer, and the results matched well [14]. Sometimes the optical detection unit is located separately from microfluidic part of the flow cytometer. Rosenauer et al. designed a single layer 3D hydrodynamic focusing miniaturized flow cytometer fabricated by standard lithography process [15]. The optical detection platform was detached from fluidic unit of the design to enhance and increase the sensitivity of optical

part. As a special feature of the fluidic chip design, a lifting port was embedded in the channel at the inlet to better hydrodynamically focus the particles. The performance and capability of the device was tested by using three different types of polystyrene beads which were different in size. The signal drop height or width was recorded on an Oscilloscope for further analysis on how much of the incident beam light was lost by the samples. The collected data showed a distinguishable arrangement of data points for 3 different populations of beads [15]. Kettlitz et al. designed, fabricated and tested a novel feature of flow cytometer using low cost and low power consumption elements. They avoided utilizing regular optics like lenses in the device; instead they used very compact and cost effective items such as LED light as light source and a PIN-photodiode as their photodetection part. Using LED instead of laser in the design provided much easier method of adjustment. Kettlitz et al. group were able to improve the limit of detection up to about 5 times by reducing the flow rate. The sensitivity in the optical detection part was also obtained by increasing the current through LED. Dichroic plastic filters had the application of filtering the wavelength of the excited light. They processed sample detection for two different high and low flow rates. It was found that for the lower sheath flow rate, the noise level was decreased and new population range of particles was able to be detected [16].

In diagnostic systems, it is important to have highly sensitive photo detector. Avalanche photo diodes (APDs) are a popular type of photo detectors. However they have a very low gain range; limited to several hundreds. Thus, APD sensitivity is not high because of the lack of internal gain. The multi-pixel photon counter (MPPC) photodetector is a new type of photodetection unit which comes with high sensitivity and gain range. It is made of thousands of APDs that are connected to each other using resistors [17].

This study presents a microfluidic flow cytometer which is equipped with a new generation of photodetectors. MPPCs are employed as part of the optical train of the system. These types of photodetectors are portable and very light gains of up to 10^7. A load resistor can set the voltage output on couple of millivolts which makes the MPPC capable of having signal photon response. High resolution and low noise level are as other important advantages of MPPCs. They are also not responsive to magnetic field and are able to detect photon packages in very small amount [17]. Multiple APDs that are working in Geiger mode give a strong resolution and great response to external light. The MPPC effective area is really small. This is why they are capable of amplifying the photocurrent on a micrometer scale of magnitude. The amplified photocurrent gives us a high sensitivity level from detection side of view. Using the MPPC modules in our optofluidic device, we are able to develop a microfluidic system that is more portable with higher resolution compared to earlier generation of flow cytometers. The details of how MPPC is able to strengthen the light input for obtaining a promising performance are explained in methods. Photons are absorbed by electrons and holes inside the MPPC. This causes charges to accelerate in a very strong electric field which is similar to what occurs in photomultipliers. Different arrays of APD photodetectors allow MPPCs to have a high gain values. Geiger mode is the situation where MPPC reversed voltage is higher than the breakdown voltage. We have employed two types of MPPCs in the optical system which differs in size of surface area and sensitivity correspondingly. Results show a high signal-to-noise ratio. A larger range of signals from samples compared to noise levels produces a promising signal distribution during the time of data acquisition. Having high sensitivity and resolution signal-to-noise ratio with considerable recorded points for each peak. The peaks include the data points for each sample that passes the interrogation region. Greater amount of points for each peak is correlated to the resolution of the

photodetector in the system. Also, MPPCs are sensitive enough to be able to received considerable number of points for each signal out. A wider peak relates to a higher sensitivity of detection unit. The main advantage of using MPPCs in our setup is to make the size of the whole system as small as possible to introduce it as a lab on a chip flow cytometer. Low power consumption is another great feature of this photodetection unit that highlights the capability of our fabricated optofluidic cytometer. Figure 13 shows the schematic of two different MPPCs with different surface areas (3x3 mm and 1x1 mm). We have employed the MPPC with larger surface area (S10362-33-100C, Hamamatsu Company, Japan) in our flow cytometer to be able to collect more light through the photodetector.

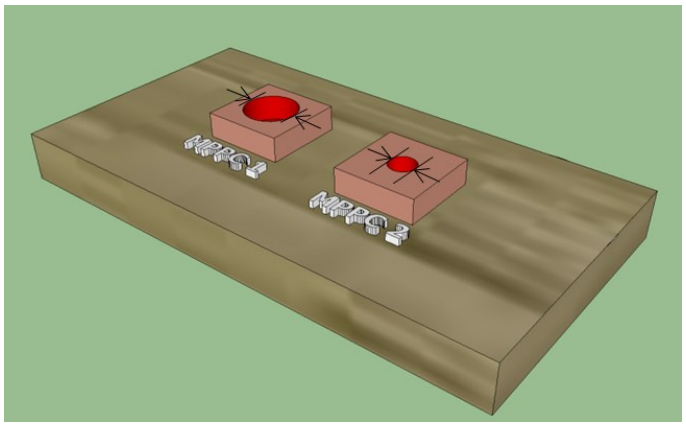

Figure 16. A schematic of two MPPCs with different surface areas of 3x3 mm and 1x1 mm. The MPPC with larger surface area (S10362-33-100C) was chosen for this design.

4.3. Materials and Methods

4.3.1. Microfluidics

The mold is fabricated using photolithography techniques and soft baking. The microchannel is made of polydimethylsiloxane (PDMS). The chip is consisted of two sheath

channels and one sample flow channel. Both sheath and sample flows are introduced into the channel using a bidirectional syringe pump (Cole-Parmer, Vernon Hills, IL) at 200 µL/min and 10 µL/min, respectively. The height and width of the channel are 130 µm and 390 µm, respectively. Arrays of chevrons are designed and fabricated on both top and bottom of the microchannel. Chevrons have 100 µm width and 65 µm height. The first sets of chevrons which are located in before the interrogation region of the microchannel are responsible for focusing the sample stream. The next arrays of chevrons (reverse chevrons) located after the interrogation region unsheathes the sample flow and return it to its original position [18]. Figure 14 shows how the core flow is compressed vertically by the arrays of chevrons. The core flow is compressed vertically and expands horizontally as it passes through the chevrons.

The core solution contains microbeads with a concentration of 50 beads per microliter. The beads are fluorescent sky blue (Spherotech Inc., Lake Forest, IL) with an excitation peak of 635 nm. Two different sizes of beads, 3.2 µm and 10.2 µm, are used to for characterization purposes.

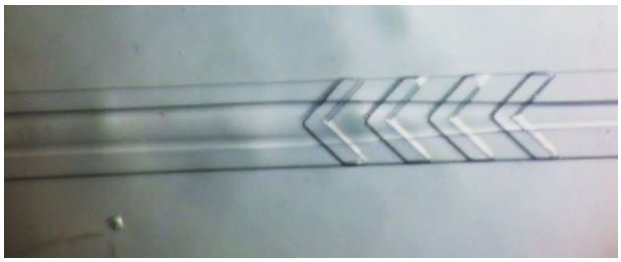

Figure 17. Optical microscopy of the chevron section. The photo shows vertical compression of the core stream as it passes through the arrays of chevrons.

3.3.2. Optics and Electronics

Multimode optical fibers (fiber instrument sales Inc., Oriskany, NY) are used as excitation and emission carriers. Fibers are inserted into the channel to excite the samples and collect scattered light. The excitation light is provided using a red laser (Laser pointer 100mW, ArmLaser, San Francisco, California) at 635 nm in wavelength. The emission fibers are perpendicular to the excitation fiber and are responsible to carry the light from microbeads to the photodetection unit of the system. The emission fibers are precisely mounted in the same plane as the excitation fiber to receive the highest intensity of light emitted from the fluorescent sky blue microbeads.

We have used a ceramic MPPC with an effective photosensitive area of 3x3 mm to detect the fluorescent light.

A data acquisition (DAQ) unit (NI USB-6351, National Instrument, Austin, TX) is used to collect the data from photodetection unit and send them to desktop computer. An analog input port of DAQ device was specified for collecting data points through three different channels by MPPCs. LabVIEW software is coupled with DAQ unit to monitor and visualize sampling process on the computer. The sampling rate was set to 100,000 samples per second on LabVIEW to make sure that enough data points are obtained from samples for further analysis. Because the current output from MPPC was a very low, an electric circuit was utilized to convert the current to voltage. Using electrical components like op-amps the output voltage from MPPCs was increased to an acceptable range for data acquisition unit. The MPPC was supplied with 70 V by a power supply (HY3005-3 DC Power Supply, San Jose, CA). A capacitor was utilized in each MPPC electrical circuit to run the voltage output with delay so the signal could be matched with the normal signal input of DAQ device. The background signal (noise) for MPPC could be

adjusted by changing the supply voltage. Using a bypass filter (700±10 nm, Thorlabs Inc., Newton, New Jersey, USA), we were able to cancel noise data points and have signal output only related to sample response. The filter was located between the emission fiber and the MPPC module.

Figure 15 illustrates the characterization process of the fluorescent beads. Figure 15a shows a schematic of the microchannel, laser and MPPC. The laser sends the beam through the excitation fiber. The fluorescent beads become excited and emit light which is collected through the emission fiber. The MPPC is located in front of emission fiber to collect the emitted light. Figure 15b and c show the COMSOL simulation of concentration distribution along the channel. The structured mesh is used to have an appropriate meshing quality on edges (figure 15b). Figure 15c shows the concentration distribution in the whole channel and also a cross section after the last chevron groove. Figure 15d is a snap shot of signal output from samples with two different sizes.

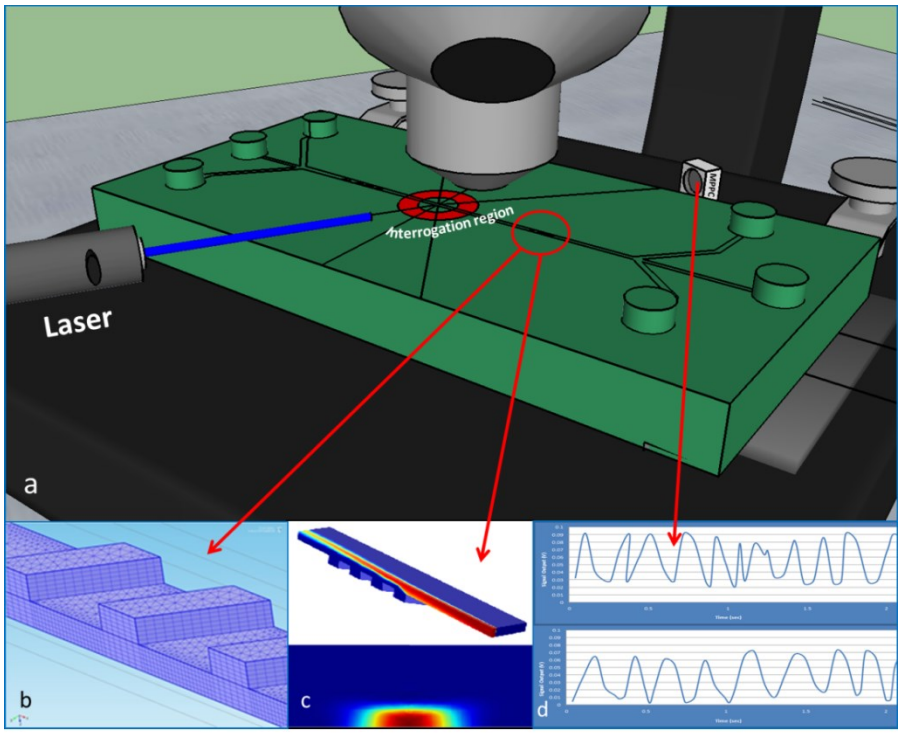

Figure 18. Characterization of microparticles using an optofluidic flow cytometer. a) A schematic of the chip under microscope. The microchannel has 3 inlets (on the left) and 3 outlets (on the right) and an interrogation region (red circle at the center). b) Structured mesh of the chevrons by COMSOL software. c) The concentration simulation shows the hydrodynamic focusing of the core stream (red) by sheath flow (blue). The cross section of the channel after the fourth chevron is also shown. d) The signal output for particles with two different sizes are presented.

4.4. Results and Discussion

4.4.1. COMSOL Modeling

COMSOL Multiphysics software is used to simulate the microchannel and confirm the results from experimental side of study. First, the geometry of the main channel is sketched in 2-dimension and it is then extruded to 3D mode. Having the 3D geometry we have to union the different elements such as chevrons and the main channel. The simulation can only be reliable if all the surfaces are connected together as a single body. Fluid properties is inserted and defined

in all surfaces of the three dimensional object. The bottom and the side walls are defined as symmetry surfaces because of symmetric geometry of the channel. This means that only fourth of the channel is simulated and analyzed by COMSOL to reduce the calculation time. Solving Navier-Stokes at steady state condition, the velocity distribution is simulated. Then, using diffusive transport, the concentration distribution along the channel is obtained. The general parameters are defined before running the program. The sheath and sample flow rates are set as 200 μL/min and 10 μL/min, respectively. The diffusivity is also fixed at $10^9 m^2/s$. As an innovative concept such as the meshing quality, structured meshing design offers the most practical method of having homogeneous pattern in all surfaces. In other words, multi pattern in meshing increases the quality of meshing and correspondingly the results are closer to reality. The horizontal and vertical surfaces have triangular and rectangular feature of meshing (figure 15c).

Due to symmetry, the velocity and concentration distribution along the channel was only simulated for half of the microchannel to decrease the computational time. The results of laminar flow simulation (velocity distribution) are used as initial condition for the transport of diluted species (concentration distribution). The concentrations of sheath and sample flow are assumed to be 0 mol/m^3 and $1 mol/m^3$, respectively.

Figure 16 shows the concentration distribution along the channel. The velocity profile was adjusted as fully developed at the entrance of the channel. Additionally, looking at the concentration simulation along the channel (Figure 16), as the core (sample) flow entered the channel (red region), it was compressed horizontally by sheath flows on both sides (a) and once the sample flow passed the chevrons, it was compressed vertically on the top and bottom. The

maximum compression in vertical direction occurred right after the last chevron (b). The concentration of the core and sheath flow flows were assumed to be 1 and 0, respectively. The quadratic solution was selected as the method of solving for fluid dynamics part of the simulation to improve the quality of the results.

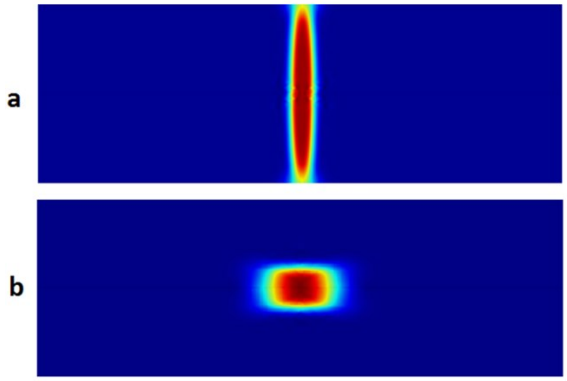

Figure 19. The concentration distribution along the channel for the cross section at: a) before the arrays of chevrons, b) after the forth chevron groove.

4.4.2. Experimental Results

Two different sizes of microspheres were assessed for forward scatter using the fabricated optofluidic cytometer. The signal output set of each MPPC was saved separately using LabView software. As we mentioned in methods, the MPPCs are different based on their surface area that is exposed to the external light. The surface area is consisted of many parallel arrays of Avalanche Photo Diodes. The MPPC with larger surface area received more packages of photons. Thus, it produced higher level of voltage output on LabView. A 700 nm bandpass filter was placed in front of each MPPC module to cut off the noise signal output for obtaining higher signal-to-noise ratio. A threshold was set to delete most of the noise responses. This is

still likely to record some noise signal output on LabView. The results showed for larger samples the width and height of the peaks were increased. The number of data points collected in each peak was dependant to the sampling rate that was set on LabView. The sampling rate was set at 100K samples per second to be able to find most of samples inside the microchannel. The experimental procedure is done using two different lasers. One is a pointer laser having 10 mW power output and the other one is a diode laser having 35 mW power output. The results of experiments using these two lasers are compared here. The dump fiber power for the 1 mW and 35 mW lasers were set at 2 uW and 800 uW. This is the power output from the optical fiber across the excitation fiber.

A MATLAB code is developed to collect specific signal outputs that are produced by samples. The code detects the peaks in the set of signals that are determined by an empirically defined threshold. The voltages greater than or equal to the threshold are saved for further analysis.

Figure 17 shows the MPPC results (signal output) for 10.2 µm and 3.2 µm microspheres. The graphs is consisted of peaks that each one indicates one bead passing through the interrogation region.

The experiment using each laser is done in three steps: first, only water is run through the microchannel and the signal output is read. Therefore, figure 17a shows the background noise of the system as the samples are not presented yet using 1 mW laser pointer. As the second step, the 3.2µm shperes are introduced in the core stream. The results (figure 17b) shows that the signal output has increased due to presence of particles at the interrogation region. Finally, the 10.2 µm beads are run in the channel. Figure 17c clearly proves that for larger sizes of samples, the signal

output would increase drastically. The larger microspheres have more surface area than the smaller ones. This causes them to emit more packages of photon through emission fiber. Thus, they have produced higher signal output than smaller particles.

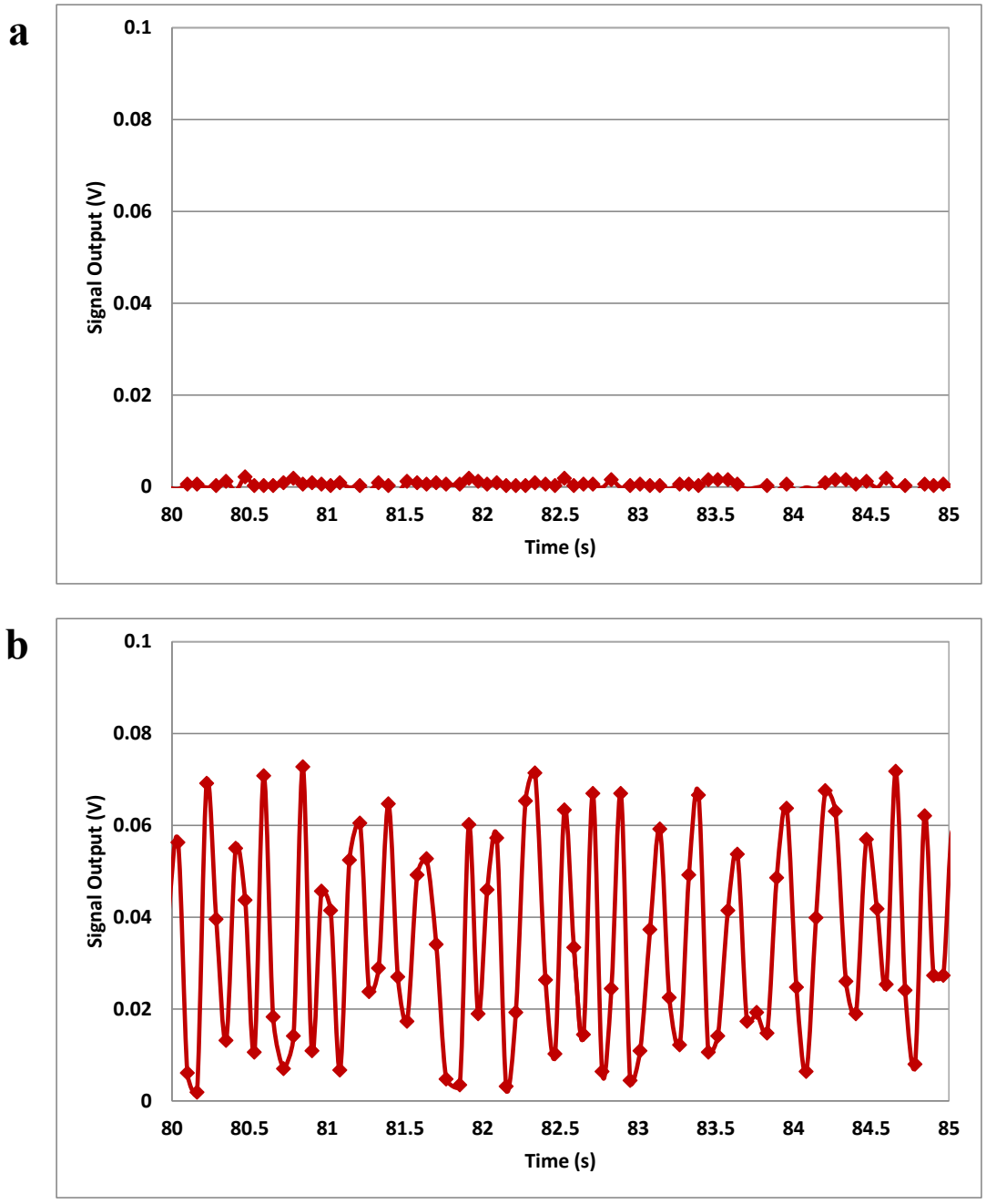

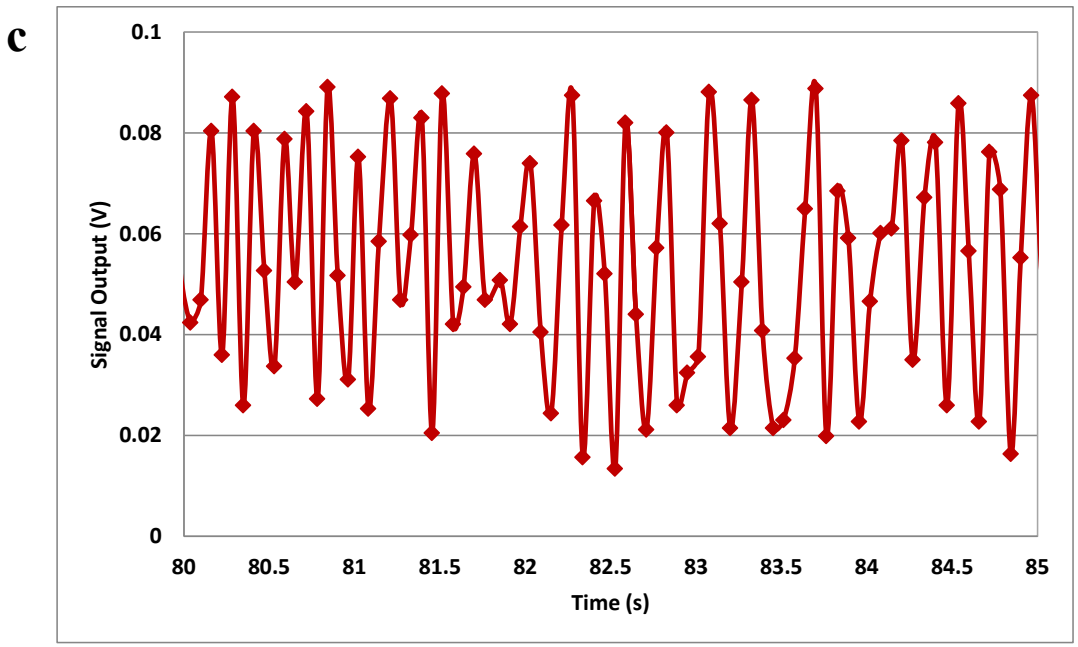

Figure 20. Signal output collected by MPPC and DAQ device for three different cases. a) Only water is pumped into the microchannel. b, c) Signal output that are received from 3.2 µm (b) and 10.2 µm (c) microspheres.

Figure 18 shows the statistical analysis for signal output collected for two different sizes of beads. The blue and red bars are the average signal output (integral of the peak) for each peak generated by each bead passing through the interogation region. The average value for 10.2 and 3.2 µm beads signals were 0.139 V and 0.089 V, respectively. The results show that for the bigger particles the average signal output is higher. The standard error for blue and red bars are 0.004 and 0.002, respectively.

Integrating 3D hydrodynamiccal focusing design and a new generation of photodetector with high sensitivity and very small footprint, we were able to succesfully detect particles as small as 3.2 µm and discriminate populations of microparticles with different sizes.

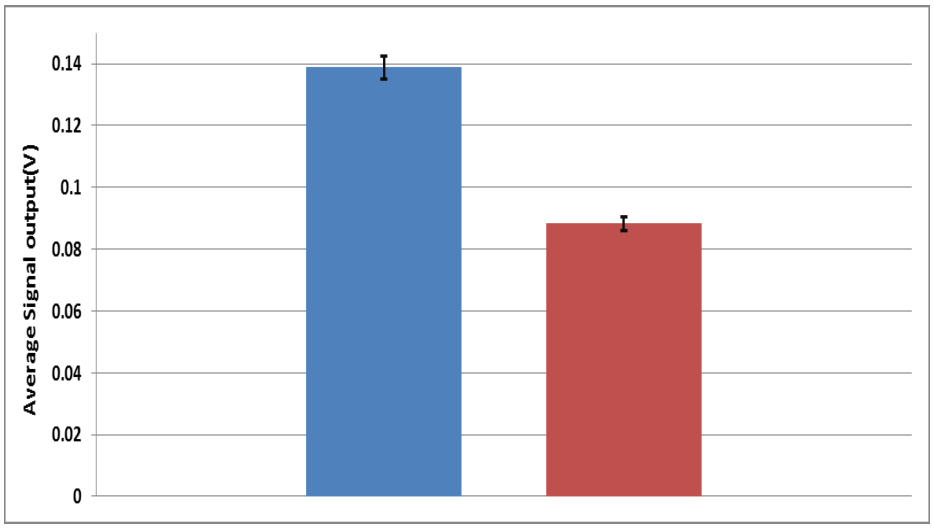

Figure 21. The statistical analysis on two different sizes of beads. The blue bar shows higher average signal output (integral of the peak) for 10.2 microns particles compared to signal output for 3.2 microns samples (red bar).

As mentioned, the same experiment is done using a more powerful diode laser with 35 mW in terms of power output. The results are going to compare with the results obtained from the laser pointer (1 mW power output). We expect to get higher signal to noise ratio for the experiement of running microspheres inside the channel.

Figures 23 and 24 show significant higher signal output for the results of both samples 3.2 and 10.2 microns beads, respectively compared to the same set of results obtained by the previous laser (1 mW laser pointer).

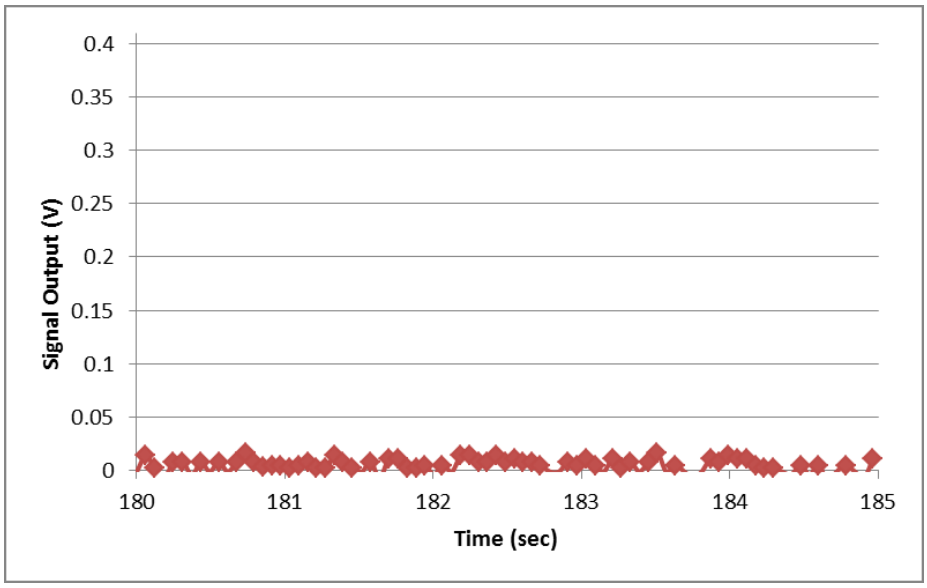

Figure 22. Signal output collected by MPPC and 35 mW diode laser for only water pumping into the micro channel.

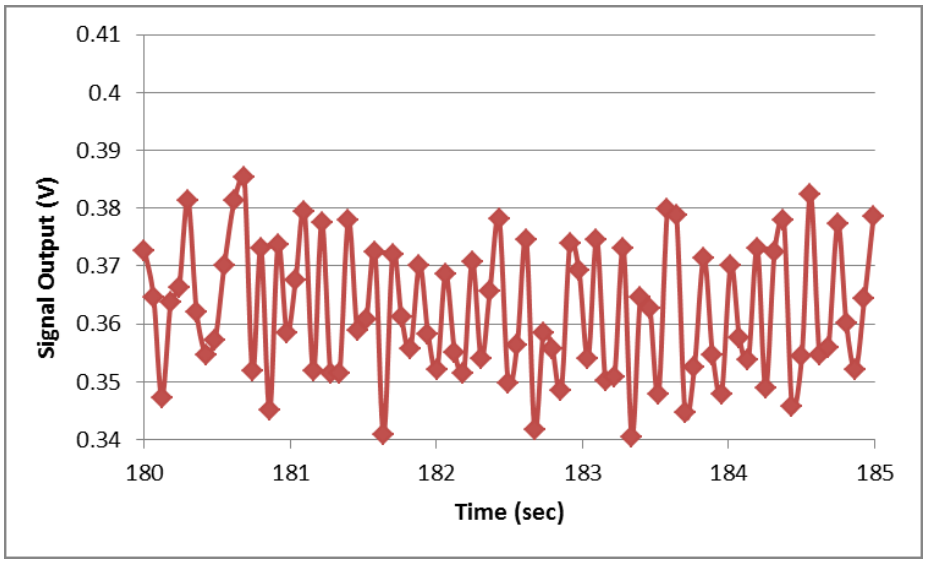

Figure 23. Signal output collected by MPPC and 35 mW diode laser for 3.2 microns microspheres running into the channel.

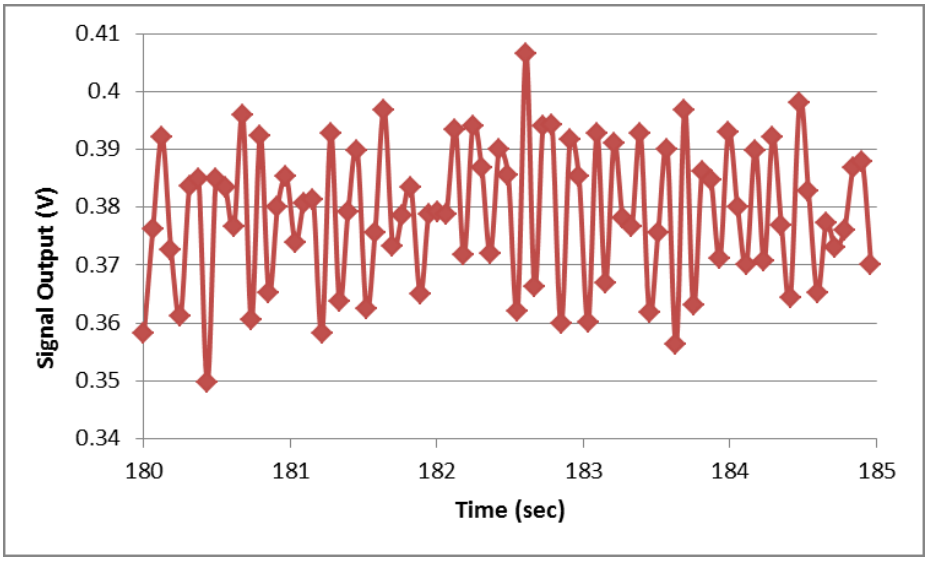

Figure 24. Signal output collected by MPPC and 35 mW diode laser for 10.2 microns microspheres running into the channel.

Figure 25 shows the statistical analysis of results using a 35 mW diode laser for both 3.2 and 10.2 microns beads. In fact, the average signal output for both samples is clearly higher than the average of signal outputs using the previous laser.

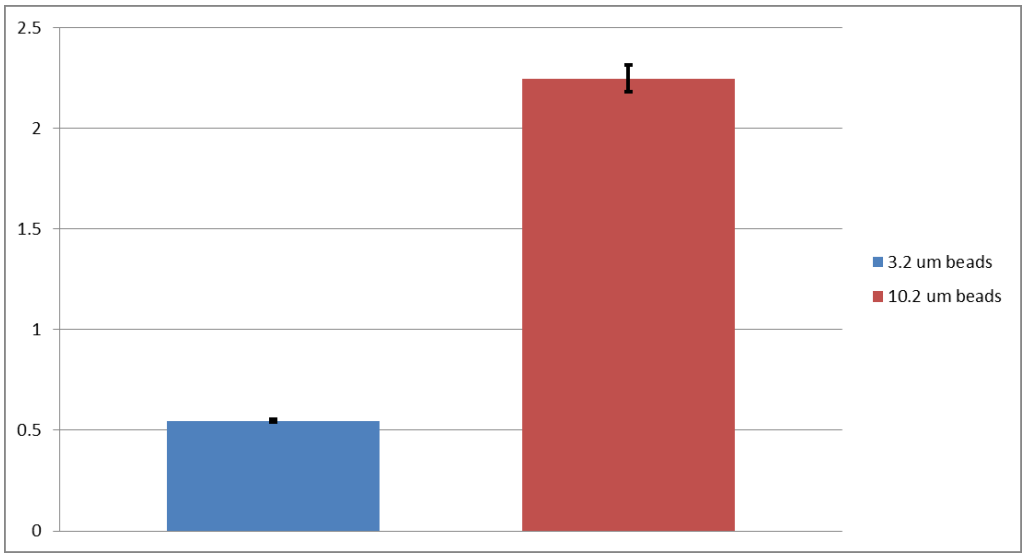

Figure 25. The statistical analysis on two different sizes of beads using 35 mW diode laser. The blue bar shows higher average signal output (integral of the peak) for 10.2 microns particles compared to signal output for 3.2 microns samples (red bar).

4.4.2.1. Cell Charactrization:

Four different types of algae are going to be run through the microchannel. They are in the range of 2 to 8 um in terms of size. The figures 19-21 show microscopy images of three types of algae. They are generally between 2-8 microns in terms of size. The algae are come in different shapes (elongated, almost spherical and tailed), so we expect to get different ranges of signal-to-noise ratio for each set of sample. The Chlamydomonas is one of the tailed algae that we expect to get clearly different signal output for this kind of algae through signal processing by our microflow cytometer.

4.4.2.1.1. Chlamydomonas Reinhardtii

This type of algae is the most popular green algae that is being used widely in laboratories. It is also called Chlorophyta. It could be found in many sources such as fresh water,

soil and oceans. This algae has a cell wall, an eye that sense the light, a chloroplast and two flagella. This type of algae could even grow on a medium of inorganic salts. Having photosynthesis processes, the energy could then be produced. Chlamydomonas has many applications in cell and molecular biology field. The motion, the response to environmental conditions and how they work could be of its many applications. Figure shows the microscopy image of this kind of algae [19].

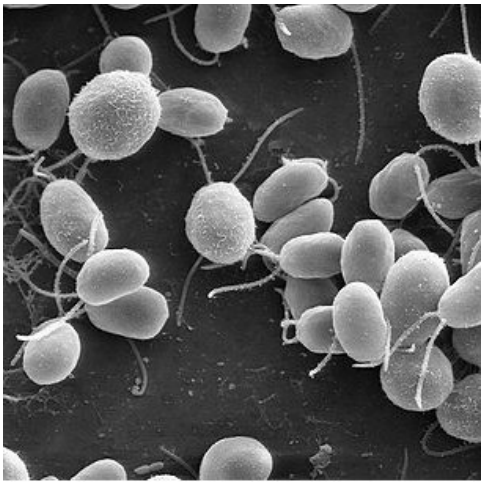

Figure 26. Chlamydomonas Reinhardtii. Microscopy image (3000X magnified)[20]

4.4.2.1.2. Nannochloropsis

This type of algae has made a considerable attraction in production of biofuels. In that application Nannochloropsis plays the role of feedstock. Nannochloropsis has a lot of amount of lipid. The lipids are used as the initial substrate for producing oil-based diesel fuel. Figure shows the microscopy image of Nannochloropsis [21].

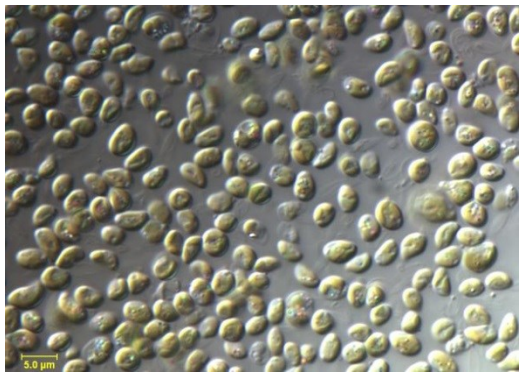

Figure 27. Nannochloropsis microscopy image[22]

4.4.2.1.3. Chorella Sorokiniana

Chorella is also another type of green microalgae that used widely to produce biodiesel fuels. This algae is one of the single celled algae that could be found in fresh water. It has a high amount of chlorophyll. This algae reproduces at a very fast rate [23].

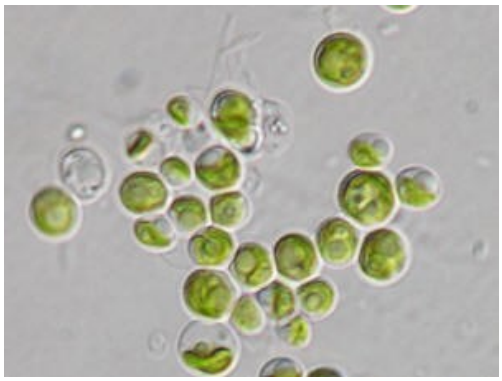

Figure 28. Chorella Sorokiniana microscopy image [24]

Using the above mentioned cells as the samples to run in the channel, we have obtained the signal output collected from three types of algae running in the microchannel. Figures 29 to 31 are the signal output for Chorella, Chlamy Su1 and Chlamy 21gr based on Voltage output

collected from the system. Signal output that received for Chorella has clearly higher magnitude compared to other two types of algae. This fact confirmed that Chorella has bigger size compared to Chlamy 21gr and Chlamy Su1. Also the slight difference in size for Chlamy 21gr and Chlamy Su1 is observable [25].

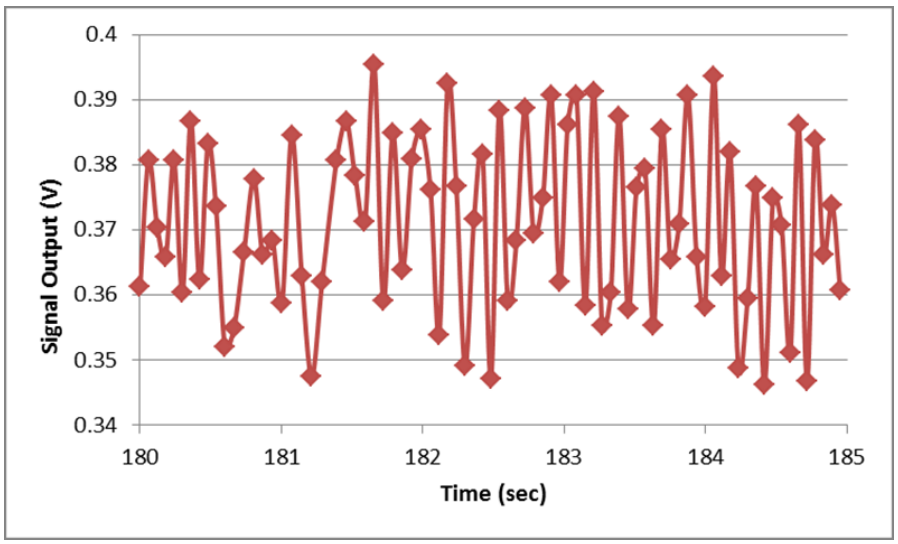

Figure 29. Signal output collected from Chorella

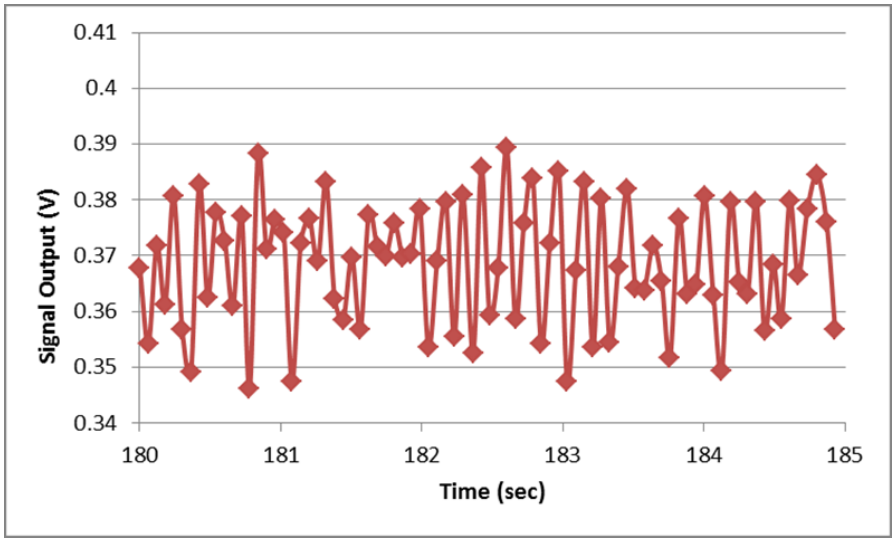

Figure 30. Signal output collected from Chlamy Su1

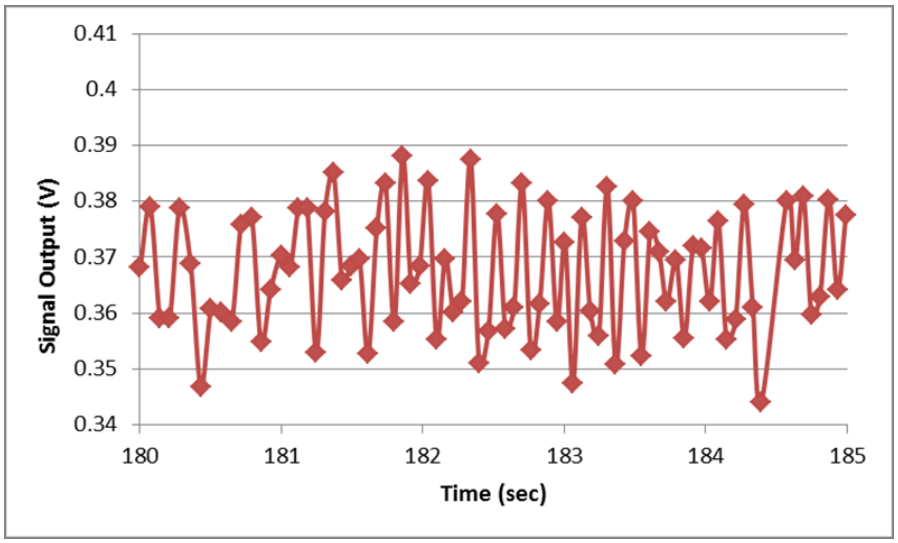

Figure 31. Signal output collected from Chlamy 21 gr

Figure 32 shows the statistical results of running the algae in the channel. It proves that for Chorella, the signal output is clearly higher than the results for Chlamy 21gr and Chlamy Su1. This means that Chorella has bigger size compared to the other two types of algae. Figure 32 also shows that Chlamy Su1 is slightly larger than Chlamy 21gr in terms of size.

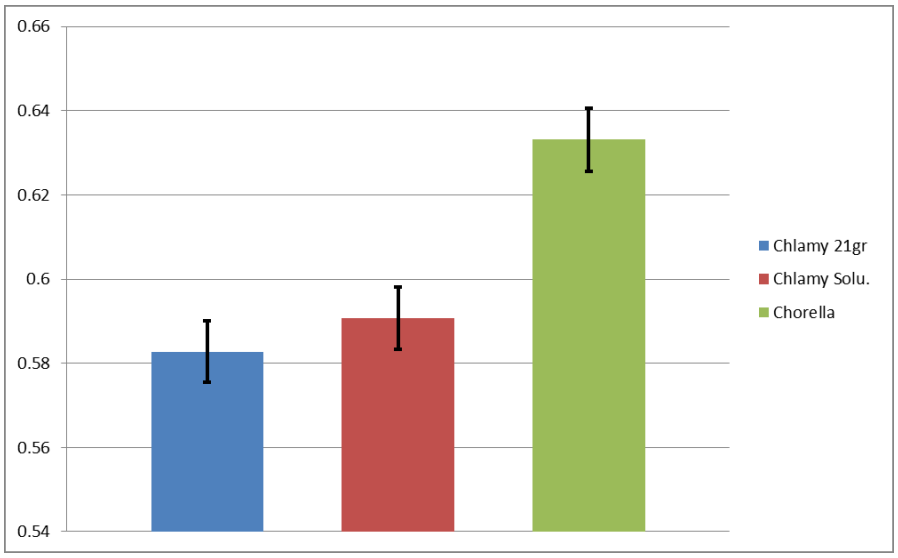

Figure 32. Signal output from three types of algae

4.4.3. Conclusions

We have fabricated and developed an optofluidic flow cytometer equipped with a multi-pixel photon counter. The high sensitivity and compact size of MPPC photodetector allowed us to detect micro-particles precisely with high gain level up to 10^7. Our fabricated flow cytometer is sensitive enough to detect particles in the range of 3 microns. The statistical analysis of different sizes of beads demonstrated significantly different signal outputs for 3.2 μm and 10.2 μm samples based on their average signal output that they had produced. For the larger spheres, higher signal output was produced. The 10.2 μm beads also resulted in higher standard errors. The new set of results obtained using a more powerful laser (35 mW diode laser) and they confirmed significantly higher signal output compared to the results of 1 mW laser pointer. COMSOL simulation results also confirmed the 3D hydrodynamic focusing of the core stream by the sheath stream and arrays of chevrons. Using a 35 mW diode laser, we were also able to characterize three tupes of algae based on their size.

4.6. References

[1] Thyssen, M., Mathieu, D., Garcia, N. and Denis, M., 2008, *J. Plankton Res.*, **9**, 1027–1040.

[2] Nastaran Hashemi, Jeffrey S. Erickson, Joel P. Golden, Kirsten M. Jackson and Frances S. Ligler, *J. Biosens. and Bioelec.*, 2011, **26**, 4263-4269.

[3] Heidi M. Dierssen, 2010, **107**, 17073-17078.

[4] P. B. Howell, J. P. Golden, L. R. Hilliard, J. S. Erickson, D. R. Mott and F. S. Ligler, *Lab Chip*, 2008, **8**, 1097–1103.

[5] X. Mao, J. R. Waldeisen, and T. J. Huang, 2007, *Lab Chip*, **10**, 1260.

[6] J. P. Golden, J. S. Kim, J. S. Erickson, L. R. Hilliard, P. B. Howell, G. P. Anderson, M. Nasir, and F. S. Ligler, 2009, *Lab Chip*, **13**, 1942.

[7] N. Hashemi, J.S. Erickson, J.P. Golden, F.S. Ligler, 2011, *Biomicrofluidics*, **5**, 032009.

[8] R. Bernini . E. De Nuccio . F. Brescia . A. Minardo . L. Zeni . P. M. Sarro . R. Palumbo . M. R. Scarfi, 2006, *Anal. Bioanal. Chem.*, **386**, 1267–1272.

[9] Guocheng Shao, Wanjun Wang, 2010, *Microsys. Technol.*, **16**, 1569-1576.

[10] G. Hairer and M. J. Vellekoop, 2009, *Microfluidic Nanoofluidic*, **5**, 647-658.

[11] Derek Tseng, Onur Mudanyali, Cetin Oztoprak, Serhan O. Isikman, Ikbal Sencan, Oguzhan Yaglidere and Aydogan Ozcan, 2010, *Lab Chip*, **10**, 1787-1792.

[12] Zhu, H., Mavandadi, S., Coskun, A.F., Yaglidere, O. and Ozcan, A. ,2011, *Anal. Chem.*, **83**, 6641-6647.

[13] S. Kostner and M.J. Vellekoop, 2008, *Sens. and Actuat. B*, **132**, 512–517.

[14] Xiaole Mao, Ahmad Ahsan Nawaz, Sz-Chin Steven Lin, Michael Ian Lapsley and Yanhui Zhao, 2012, *Biomicrofluidics*, **6**, 024113.

[15] Michael Rosenauer , Wolfgang Buchegger, Inez Finoulst, Peter Verhaert and Michael Vellekoop, 2011, *Microfluid Nanofluid*, **10**, 761–771.

[16] Siegfried W. Kettlitz, Sebastian Valouch, Wiebke Sittel and Uli Lemmer, 2012, *Lab Chip*, **12**, 197–203.

[17] Zhang, Guoqing, Yu, Changfeng, Zhu, Changjun, Liu, Lina, 2013, *Optik – Inter. J. for Light and Elec. Optics*, **124**, 5781– 5786.

[18] N. Hashemi, P.B. Howell, J.S. Erickson, J.P. Golden, and F.S. Ligler, 2010, *Lab Chip*, **10**, 1952-1959.

[19] http://en.wikipedia.org/wiki/Chlamydomonas_reinhardtii

[20] http://botany.natur.cuni.cz/algo/CAUP/H1986_Chlorella_sorokiniana.htm

[21] http://cfb.unh.edu/phycokey/Choices/Eustigmatophyceae/NANNOCHLOROPSIS/ Nannochloropsis_Image_page.html

[22] http://www.nannochloropsis.org/

[23] http://www.oilgae.com/ref/glos/chlorella_sorokiniana.html

[24] http://www.chlamy.org/info.html

[25] http://www.cder.dz/download/Art14-1_3.pdf

CHAPTER 5. CONCLUSION

5.1. Conclusion

In this study, development of an optofluidic system using MPPC photodetector presented. The results showed a significant higher signal output for larger samples using the multi-pixel photon counter. It was utilized as the main part of the photo detection unit of the system. Having high resolution and high sensitivity with compact size motivated us to employ this type of photodetector into the setup. MPPCs sent out the signals in a fast sampling rate (100K samples per seconds) since they were consisted of many arrays of avalanche photo diodes. Two different lasers were included in the system to investigate the effect of power output of lasers on signal output obtained from the samples.

COMSOL software was also used to simulate the channel and obtain the results for velocity and concentration distribution along the channel. Only one-fourth of the channel was designed on COMSOL to lower the time of calculations. Both velocity and concentration results were obtained by defining the flow in laminar condition. The velocity distribution clearly proved increasing the velocity within the chevron grooves. The concentration distribution also showed how the chevrons compressed the core flow from the top and the bottom of the channel. Compressed core flow from sides was also detectable by the concentration distribution. In fact, 3D dynamically focusing property of the flow was proved by the COMSOL results.

5.2. Future Work

As the future work, a microfluidic chip is going to be attached to the flow cytometer which is equipped with an ionic electroactive actuator. An integrated microfluidic chip is developed which utilizes ionic electroactive polymer (IEAP) actuators as artificial cilia to achieve active microfluidic mixing. A thin polyethylene sleeve designed to protect the actuators inside the microchannel. The microchannel is again fabricated in PDMS. In addition, our IEAP actuators are relatively easy to fabricate compared with some of the more complex microfabrication techniques necessary to produce the artificial cilia found in other mixing devices. These actuators are also characterized as having a relatively fast response time, high strain, and high efficiency [1, 2]. However, the most important advantage is the low operating voltage; these actuators are typically run at less than 5 V. Since the ultimate goal of much of microfluidic development is to produce a portable lab-on-a-chip device, low power solutions are critical to each function that will be integrated on the chip. The proof-of-concept experiments showed that the actuators are capable of mixing laminar fluid flow. Our device is designed to be integrated with an existing microflow cytometer [3, 4] as a sample pre-processing step, and with further optimization and engineering could easily become a viable alternative to other mixing methods. Finally we are going to do some sorting and concentrating the cells inside the channel with utilizing the IEAP equipped chip coupled with our fabricated microflow cytometer.

5.3. References

[1] Montazami, R., et al., Thickness dependence of curvature, strain, and response time in ionic electroactive polymer actuators fabricated via layer-by-layer assembly. Journal of Applied Physics, 2011. 109: p. 104301.

[2] Montazami, R., D. Wang, and J.R. Heflin, Influence of conductive network composite structure on the electromechanical performance of ionic electroactive polymer actuators. International Journal of Smart and Nano Materials, 2012. 3(3): p. 204-213.

[3] Hashemi, N., et al., Optofluidic characterization of marine algae using a microflow cytometer. Biomicrofluidics, 2011. 5: p. 032009.

[4] Hashemi, N., et al., Microflow Cytometer for optical analysis of phytoplankton. Biosensors and Bioelectronics, 2011. 26(11): p. 4263-4269.